THE JOURNAL OF BIOLOGICAL CHEMISTRY VOL. 286, NO. 26, pp. 22991–23002, July 1, 2011

N-Linked Glycosylation Regulates Human Proteinase-activated Receptor-1 Cell Surface Expression and Disarming via Neutrophil Proteinases and Thermolysin

Received for publication, November 18, 2010, and in revised form, April 17, 2011 Published, JBC Papers in Press, May 6, 2011, DOI 10.1074/jbc.M110.204271

Yu Pei Xiao, Alyn H. Morice, Steven J. Compton, and Laura Sadofsky[1]

From the Division of Cardiovascular and Respiratory Studies, University of Hull, Hull York Medical School, East Yorkshire, HU16 5JQ, United Kingdom

Proteinase-activated receptor 1 (PAR_1) induces activation of platelet and vascular cells after proteolytic cleavage of its extracellular N terminus by thrombin. In pathological situations, other proteinases may be generated in the circulation and might modify the responses of PAR_1 by cleaving extracellular domains. In this study, epitope-tagged wild-type human PAR_1 ($hPAR_1$) and a panel of *N*-linked glycosylation-deficient mutant receptors were permanently expressed in epithelial cells (Kirsten murine sarcoma virus-transformed rat kidney cells and CHO cells). We have analyzed the role of *N*-linked glycosylation in regulating proteinase activation/disarming and cell global expression of $hPAR_1$. We reported for the first time that glycosylation in the N terminus of $hPAR_1$ downstream of the tethered ligand (especially Asn^{75}) governs receptor disarming to trypsin, thermolysin, and the neutrophil proteinases elastase and proteinase 3 but not cathepsin G. In addition, $hPAR_1$ is heavily *N*-linked glycosylated and sialylated in epithelial cell lines, and glycosylation occurs at all five consensus sites, namely, Asn^{35}, Asn^{62}, Asn^{75}, Asn^{250}, and Asn^{259}. Removing these *N*-linked glycosylation sequons affected $hPAR_1$ cell surface expression to varying degrees, and *N*-linked glycosylation at extracellular loop 2 (especially Asn^{250}) of $hPAR_1$ is essential for optimal receptor cell surface expression and receptor stability.

Proteinases can exert many biological effects on cells by virtue of their ability to cleave a plethora of protein substrates. Our understanding of proteinase signaling has advanced since the discovery of a small family of G protein-coupled receptors termed proteinase-activated receptors (PARs)[2] (1–3). Classically, thrombin activates PAR_1 by proteolytic cleavage of the PAR_1 N-terminal domain between Arg^{41} and Ser^{42} to expose a new N terminus that acts as a tethered ligand and subsequently triggers receptor activation (2). Thrombin is a serine proteinase generated at the sites of vascular injury during the coagulation cascade and activates various types of cells in the vasculature like platelets and endothelial cells (2, 3). In addition to thrombin, other proteinases may be generated in the circulation under pathological situations; any proteinase that cleaves the correct peptide bond within the N terminus of PAR_1 may be able to expose the tethered ligand and then initiate intracellular signaling to provoke a cellular response (1, 2, 4–8). Conversely, proteinases can also disarm PAR_1 by proteolytic removal of the tethered ligand domain from the receptor (4, 9–14). Such disarmed receptors remain at the cell surface but are no longer available for activation by activating proteinases (*e.g.* thrombin); they can, however, be activated by the corresponding PAR_1 activating peptides (1, 2, 15). Moreover, some of those proteinases (*e.g.* trypsin and neutrophil proteinases) have been reported to activate and/or disarm PAR_1 in different cell systems (2, 4, 8, 13, 14, 16–18). Activation and desensitization of PAR_1 must be well controlled in order to eliminate the potential pathological damage resulting from unchecked receptor signaling (14).

Our previous pharmacological studies have reported that activation of $hPAR_2$ by mast cell tryptase can be regulated by receptor N-terminal glycosylation (19, 20). To our knowledge, $hPAR_1$ contains a total of five predicted sites for *N*-linked glycosylation; three sequons are located on the receptor N terminus (Asn^{35}-Ala^{36}-Thr^{37}, Asn^{62}-Glu^{63}-Ser^{64}, and Asn^{75}-Lys^{76}-Ser^{77}), and two are located within extracellular loop 2 (ECL2; Asn^{250}-Ile^{251}-Thr^{254}, and Asn^{259}-Glu^{260}-Thr^{261}) (Fig. 1) (21). PAR_1, downstream of the tethered ligand, possesses two *N*-linked glycosylation sequons (Asn^{62} and Asn^{75}), which are located along the N terminus in a domain where disarming proteinases may target. In addition, previous studies demonstrated that thermolysin and neutrophil proteinases target specific sites that are close proximally to these glycosylation sequons (Fig. 1) (12, 13, 16). Hence, we have analyzed the role of *N*-linked glycosylation in regulating cell surface expression and proteinase activation/disarming of $hPAR_1$. We have permanently expressed epitope-tagged wild-type or glycosylation-deficient mutant $hPAR_1$ in KNRK and CHO (Pro5 and Lec2) cell lines and sought to determine (i) the influence of *N*-linked glycosylation sequons on the receptor cell surface expression and signaling and (ii) the role of N-terminal glycosylation sequons, especially Asn^{62} and Asn^{75}, in regulating receptor signaling by neutrophil proteinases and thermolysin.

EXPERIMENTAL PROCEDURES

Materials—DMEM, sodium pyruvate, penicillin, streptomycin, amphotericin B, heat-inactivated FCS, non-enzymic cell dissociation solution, Geneticin (G418), Opti-MEM medium,

[1] To whom correspondence should be addressed. E-mail: L.R.Sadofsky@Hull.ac.uk.

[2] The abbreviations used are: PAR, proteinase-activated receptor; $hPAR_1$, human proteinase-activated receptor-1; KNRK, Kirsten murine sarcoma virus-transformed rat kidney; eYFP, enhanced yellow fluorescent protein; $hPAR_1E$, human proteinase activated receptor-1 with eYFP tag; ECL2, extracellular loop 2; HUVEC, human umbilical vein endothelial cell; N35–259Q, N35Q/N62Q/N75Q/N250Q/N259Q mutant.

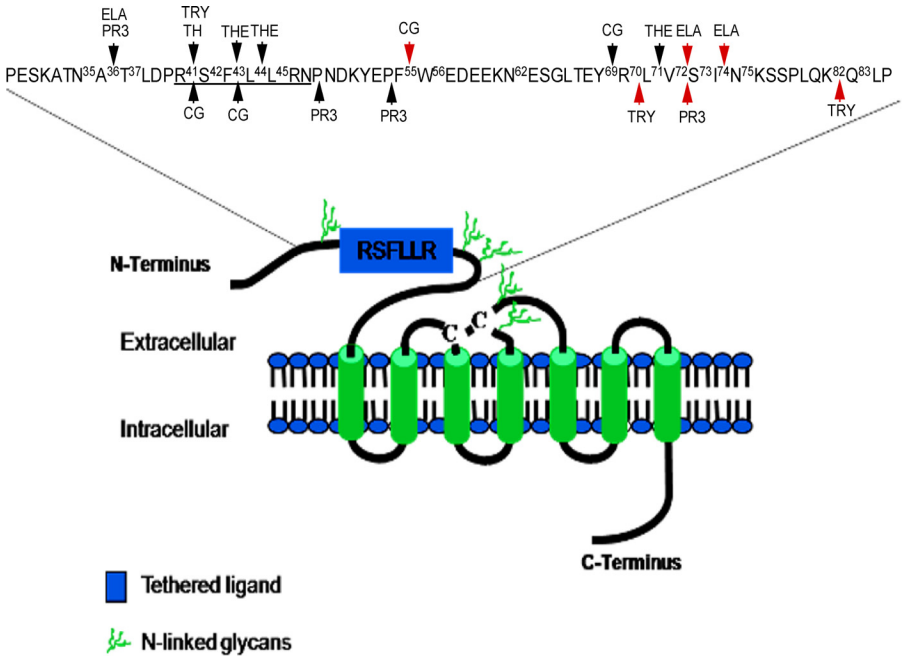

FIGURE 1. **Representative model of hPAR$_1$ displaying the five potential *N*-linked glycosylation sequons and potential proteinase cleavage sites at the extracellular N terminus.** Three sequons are located on the receptor N terminus (Asn^{35}-Ala^{36}-Thr^{37}, Asn^{62}-Glu^{63}-Ser^{64}, and Asn^{75}-Lys^{76}-Ser^{77}) and two are located within extracellular loop 2 (ECL2; Asn^{250}-Ile^{251}-Thr^{254} and Asn^{259}-Glu^{260}-Thr^{261}). Of the sequons at the N terminus, one (Asn^{35}-Ala^{36}-Thr^{37}) is located N-terminal of the cleavage/activation site (R^{41} ↓ S^{42}FLLR), and the remaining two (Asn^{62}-Glu^{63}-Ser^{64} and Asn^{75}-Lys^{76}-Ser^{77}) are located downstream of the cleavage/activation site. The disulfide bridge is shown by the two cysteines (C-C). The *red arrows* indicate the preferential cleavage site for each proteinase. *TH*, thrombin; *TRY*, trypsin; *THE*, thermolysin; *PR3*, proteinase 3; *CG*, cathepsin G; *ELA*, elastase. This figure was adapted from Refs. 4, 12, 13, and 29.

Lipofectamine 2000, dNTPs, oligo(dT)$_{12-18}$ primer, AccuPrime DNA polymerase, and Fluo-3 acetoxymethyl ester were all purchased from Invitrogen. Primers were designed "in house" and purchased from MWG-Biotech (Ebersberg, Germany). PCR purification kits, gel extraction kits, and plasmid isolation kits were all bought from Qiagen (Crawley, UK). XL1-Blue supercompetent cells and the QuikChange® site-directed mutagenesis kit were purchased from Stratagene Europe (Amsterdam, The Netherlands). The rapid DNA ligation kit was bought from Roche Applied Science. All restriction enzymes were purchased from New England Biolabs (Hitchin, UK). Anti-PAR$_1$ ATAP-2 monoclonal antibody was purchased from Zymed Laboratories Inc. (San Francisco, CA). PAR$_1$ activating peptide TFLLR-NH$_2$ was purchased from Peptides International. Enhanced yellow fluorescent protein (eYFP) was obtained from BD Biosciences Clontech. Proteinase 3 was obtained from Athens Research and Technology, Inc. (Athens, Greece). Human leukocyte elastase and cathepsin-G were purchased from Elastin Products Co. Inc. M-Per mammalian protein extraction reagent and the ProFound HA.11 immunoprecipitation kit were purchased from Pierce. All other chemicals and reagents were purchased from Sigma-Aldrich unless otherwise stated.

Generation of cDNAs Encoding WT hPAR$_1$E—Using an overlapping PCR approach, eYFP was fused to the C terminus of WT hPAR$_1$ (pro-opiomelanocortin-M1-hPAR$_1$-HA.11 in pcDNA3.1; C-terminally tagged with an HA.11 epitope and N-terminally tagged with an M1 epitope and a pro-opiomelanocortin) to generate WT hPAR$_1$E (pro-opiomelanocortin-M1-hPAR$_1$-HA.11-eYFP). The WT hPAR$_1$E was subsequently amplified and purified and then sequenced by MWG-Biotech.

Generation of Glycosylation-deficient Mutant Cell Lines—All glycosylation-deficient mutants were generated using the QuikChange® site-directed mutagenesis kit and confirmed by MWG-Biotech sequencing. The oligonucleotides were designed to replace the asparagine residues at positions Asn^{35}, Asn^{62}, Asn^{75}, Asn^{250}, and Asn^{259} with glutamine residues. Single-site mutants (N35Q, N62Q, N75Q, N250Q, and N259Q) were first constructed. In order to elucidate the cumulative effects of a lack of glycosylation at multiple sites, four receptors with multiple glycosylation mutations (N62Q/N75Q, N35Q/N62Q/N75Q, N250Q/N259Q, and N35–259Q) were constructed. In addition, the alanine mutations were created at amino acid positions Phe^{55}-Trp^{56} or Val^{72}-Ser^{73} of N62Q/N75Q to generate cathepsin G mutant (F55A/W56A) or proteinase 3 mutant (V72A/S73A). KNRK and CHO cells permanently expressing wild-type or mutant hPAR$_1$ cell lines were generated and cultured as described previously (Table 1) (19, 20).

Flow Cytometry Analysis (FACS)—WT and mutant cell lines (~90% confluence) with matched receptor expression were selected and used for further studies by FACS (BD Biosciences) as we described previously (19). The anti-PAR$_1$ ATAP-2 monoclonal antibody (1 μg/ml) and anti-mouse FITC-conjugated antibody (1:1000 dilution) were applied to assess the levels of receptor cell surface expression. The data were expressed as the median fluorescence of positive minus the median fluorescence of the EV (pcDNA3.1 transfected KNRK) cells.

Confocal Microscopy Analysis—For the WT hPAR$_1$eYFP and mutant cell lines, the light emitted by the eYFP (530 nm) fused to the receptor was used to assess receptor expression. Cells on coverslips were fixed by incubation in formaldehyde (3%) in

TABLE 1

KNRK and CHO fibroblast (Pro5 and Lec2) permanently expressing wild type (top) or *N*-linked glycosylation mutant (bottom) hPAR$_1$ cell clones generated for this study

In order to obtain permanent receptor-expressing cell lines, cells expressing high levels of hPAR$_1$ were isolated by FACS using the ATAP-2 anti-PAR$_1$ antibody. The glycosylation mutants were named with an N followed by a number related to the relative position of the potential glycosylation site and a Q. The alanine mutations were created at amino acid position Phe^{55}-Trp^{56} or Val^{72}-Ser^{73} of N62Q/N75Q to generate cathepsin G mutant (F55A/W56A) or proteinase 3 mutant (V72A/S73A).

Name of clone	Receptor cell surface expression level	Cell type
WT	Maximum level of WT hPAR$_1$ cell surface expression	KNRK and CHO
WT hPAR$_1$E	Maximum level of WT hPAR$_1$E cell surface expression	KNRK and CHO
WT-H	Higher level of WT hPAR$_1$ cell surface expression	KNRK
WT-M	Medium level of WT hPAR$_1$ cell surface expression	KNRK
WT-L	Low level WT hPAR$_1$ cell surface expression	KNRK
Name of clone	**Consensus sequence(s) disrupted**	**Cell type**
N35Q	Asn^{35}	KNRK
N62Q	Asn^{62}	KNRK
N75Q	Asn^{75}	KNRK
N250Q	Asn^{250}	KNRK
N259Q	Asn^{259}	KNRK
N62Q/N75Q	Asn^{62} and Asn^{75}	KNRK
N35Q/N62Q/N75Q	Asn^{35}, Asn^{62}, and Asn^{75}	KNRK
N250Q/N259Q	Asn^{250} and Asn^{259}	KNRK
N35–259Q	Asn^{35}, Asn^{62}, Asn^{75}, Asn^{250}, and Asn^{259}	KNRK
N35QhPAR$_1$E	Asn^{35}	KNRK
N62Q/N75QhPAR$_1$E	Asn^{62} and Asn^{75}	KNRK
N250Q/N259QhPAR$_1$E	Asn^{250} and Asn^{259}	KNRK
N35–259QhPAR$_1$E	Asn^{35}, Asn^{62}, Asn^{75}, Asn^{250}, and Asn^{259}	KNRK
Cathepsin G mutant	Asn^{62} , Asn^{75}, Phe^{55}, and Trp^{56}	KNRK
Proteinase 3 mutant	Asn^{62}, Asn^{75}, Val^{72}, and Ser^{73}	KNRK

PBS for 15 min at room temperature and then permeabilized in PBS containing 0.2% Triton X-100 for 10 min at room temperature. The coverslips were then mounted with anti-fade and fixed to slides. The cells were visualized by a Nikon Eclipse (TE2000-E) microscope with a Bio-Rad Radiance 2100 scanning system and lasers.

Western Blot Analysis—HA.11-tagged wild-type and glycosylation-deficient mutants of hPAR$_1$E were immunoprecipitated using a ProFound HA.11 immunoprecipitation kit as per the manufacturer's protocol. Protein samples (20 μg) were separated on a 10% SDS-polyacrylamide gel before transfer to Hybond C PVDF membrane. The membrane was subsequently blocked with PBS containing 5% nonfat milk before incubation overnight at 4 °C with the mouse monoclonal HA.11 antibody (1:1000 dilution in PBS/Tween 20 (0.1%) containing 2% nonfat milk). Blots were washed with PBS/Tween 20 (0.1%) for 1 h, replacing the buffer every 15 min, before a final incubation with the peroxidase-conjugated goat anti-mouse IgG (1:4000 in PBS/Tween 20 (0.1%) containing 2% nonfat milk) for 1 h. Following a further wash in PBS/Tween 20 (0.1%) for 1 h, bands were visualized using ECL (Amersham Biosciences).

Calcium Signaling Assay—The calcium signaling assay was performed as we described previously (19). Functional receptor activity was assessed by challenging cells with the PAR$_1$ activating peptide TFLLR-NH$_2$ (100 μM) and thrombin (5 nM). To assess whether a test proteinase was amputating the tethered ligand from the receptor (disarming), cells were first challenged by the addition of the test proteinase for 2 min. Successful amputation of the tethered ligand was then monitored by a subsequent application of thrombin (5 nM). The calcium signal in response to thrombin will be ablated if the tethered ligand has been removed from the receptor by the test proteinase. To demonstrate that the disarmed PAR$_1$ is still functional and present at the cell surface, 100 μM TFLLR-NH$_2$ was applied after thrombin challenge. A calcium signal triggered by the TFLLR-NH$_2$ is indicative of a functional PAR$_1$ at the cell surface, which is unresponsive to thrombin.

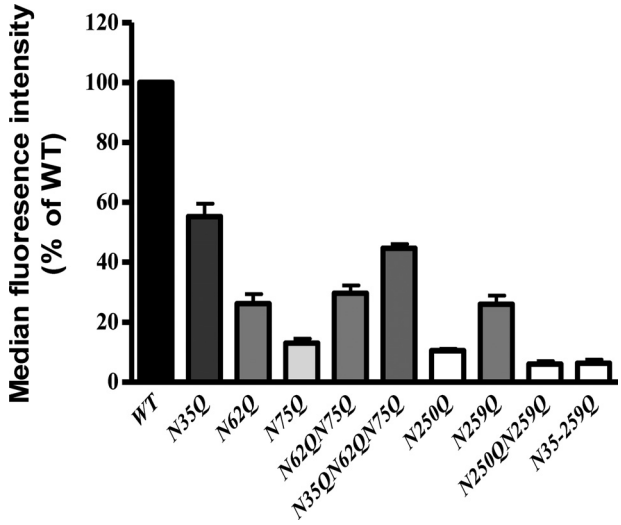

FIGURE 2. **Cell surface expression of WT hPAR$_1$ (*WT*) and glycosylation-deficient mutant hPAR$_1$ receptor in KNRK cells assessed by FACS.** Cells at ~90% confluence were harvested and incubated with the ATAP-2 antibody before incubation with an anti-mouse FITC-conjugated antibody. Results are expressed as a percentage of the median fluorescence obtained with WT hPAR$_1$ cells. The *bars* represent mean ± S.E. (*error bars*) of measurements for three independent experiments. The overall comparison showed that there were significant differences between 10 groups ($p < 0.0001$). Tukey's multiple comparison test indicated that the cell surface expression of all of the mutant receptors was significantly different from WT hPAR$_1$ ($p < 0.001$).

Calculations and Statistical Analysis—Data were analyzed using GraphPad Prism software. Statistical tests were carried out depending on the specifics of the data sets to be compared. When two cell lines subjected to the same treatment were compared, a paired Student's *t* test was adopted. The comparison of a group of cell lines subjected to the same treatment was performed by one-way analysis of variance followed by Tukey's multiple comparison test. In order to assess the changes over a period of time using a specific treatment or to assess a change over a concentration range between two different cell lines, two-way analysis of variance tables were adopted.

RESULTS

N-Linked Glycosylation at Specific Sites Regulates hPAR$_1$ Cell Surface Expression—FACS demonstrated that removing any of the glycosylation sequons resulted in a significant decrease ($p < 0.001$) in hPAR$_1$ cell surface expression in KNRK cells (Fig. 2). N35Q displayed the greatest cell surface expression; N250Q displayed the lowest expression when compared with the other single mutants, N35Q, N62Q, N75Q, N250Q, and N259Q (percentage relative to WT ± S.E.: 55 ± 4, 26 ± 3, 13 ± 1.5, 10.5 ± 0.7, and 26 ± 3% ($n = 3$) respectively). Removal of both glycosylation sequons on ECL2 (N250Q/N259Q) resulted in nearly total loss of cell surface expression (percentage relative to WT ± S.E.: 6 ± 1% ($n = 3$)). In contrast, removing all glycosy-

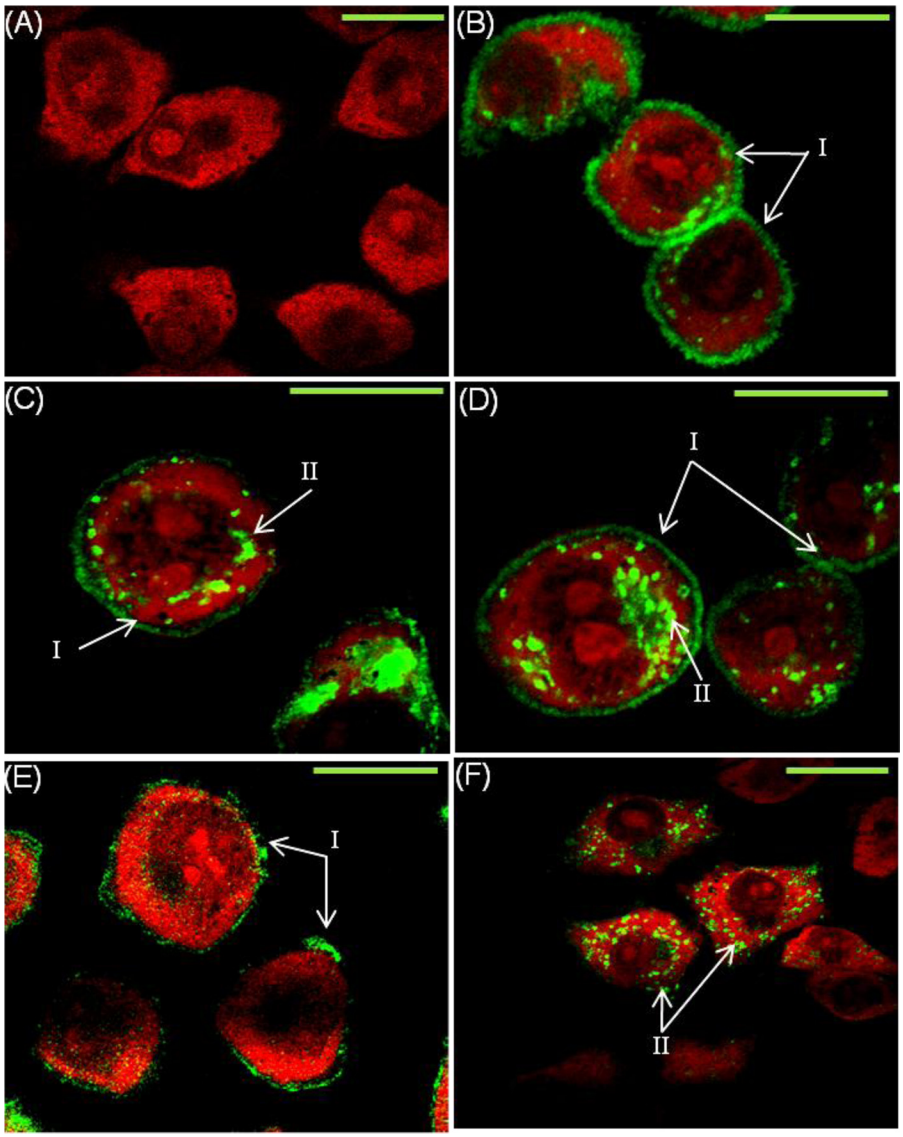

FIGURE 3. **Confocal microscopy for WT hPAR$_1$E and glycosylation-deficient mutants in KNRK cells.** eYFP-tagged PAR$_1$-expressing KNRK cells were grown on coverslips before fixing and permeabilizing. Cells were stained with propidium iodide prior to visualizing. eYFP is visualized here in *green* and propidium iodide in *red*. *I*, cell surface expression; *II*, internal receptor expression. *Green bar* on the *right* of each *panel*, 10 μm. *A*, EV; *B*, WT hPAR$_1$E; *C*, N35QhPAR$_1$E; *D*, N62Q/N75QhPAR$_1$E; *E*, N250Q/N259QhPAR$_1$E; *F*, N35–259QhPAR$_1$E. The images are representative of four independent experiments.

lation sequons on the N terminus (N35Q/N62Q/N75Q) still resulted in nearly 50% cell surface expression compared with WT expression (percentage relative to WT ± S.E.: 44.7 ± 1% (n = 3)). Removing all glycosylation sequons resulted in a receptor (N35–259Q) that was expressed at a level similar to that of the N250Q/N259Q mutant (percentage relative to WT ± S.E.: 6 ± 1% (n = 3)).

Analysis of eYFP-tagged hPAR$_1$ localization in permeabilized cells by confocal microscopy demonstrated that all hPAR$_1$E types (WT and glycosylation-deficient mutant hPAR$_1$) with the exception of N35–259QhPAR$_1$E were expressed on the cell surface; however, different levels of membrane localization and cytosolic retention were observed (Fig. 3). There was no detectable fluorescence (eYFP signaling) observed in EV cells (Fig. 3*A*). WT hPAR$_1$E displayed strong cell membrane expression with little receptor observed in the cytoplasm (Fig. 3*B*). Removal of sequon Asn^{35} in the receptor N terminus resulted in the appearance of receptor within the cytosol (Fig. 3*C*). Removal of both sequons (Asn^{62} and Asn^{75}) after the tethered ligand of hPAR$_1$ resulted in a large amount of receptor being found in the cytosol (Fig. 3*D*). The relative intensity of the receptor membrane localization and global cellular distribution appeared to be reduced significantly after removal of ECL2 glycosylation sequons (Asn^{250} and Asn^{259}) (Fig. 3*E*). Removal of all hPAR$_1$ glycosylation sequons (Asn^{35}, Asn^{62}, Asn^{75}, Asn^{250}, and Asn^{259}) resulted in a dramatic loss of cell surface expression with the highest level of receptor cytosolic retention (Fig. 3*F*).

hPAR$_1$ Is a Heavily Glycosylated and Sialylated Receptor—All of the glycosylation-deficient mutant receptors displayed different degrees of loss in molecular mass; no bands were detected in EV cells (Fig. 4*A*). The molecular mass of WT hPAR$_1$E migrated as a broad band ranging from ~37 to ~250 kDa, with the majority of the receptor being observed from ~75 to ~220 kDa. This is a pattern similar to that of N62QhPAR$_1$E.

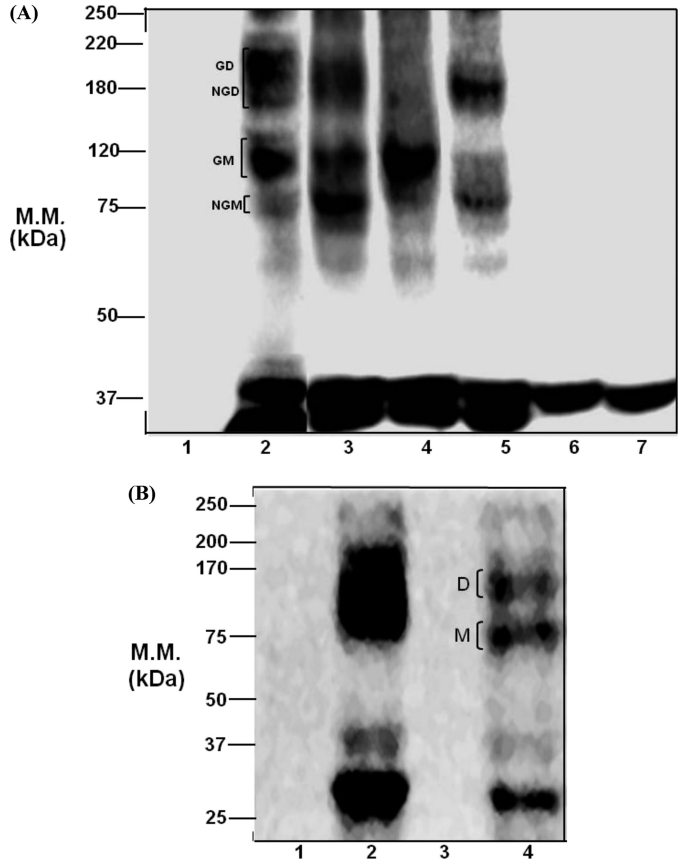

FIGURE 4. **Western blot analysis for wild-type and glycosylation-deficient mutant hPAR$_1$.** *A*, immunoprecipitates from KNRK cell lines expressing HA.11-tagged hPAR$_1$ with the potential *N*-linked glycosylation sequons removed were analyzed by SDS-PAGE (10% gel) and immunoblotted using HA.11 monoclonal antibody. *Lane 1*, EV; *lane 2*, WT hPAR$_1$E; *lane 3*, N62QhPAR$_1$E; *lane 4*, N62Q/N75QhPAR$_1$E; *lane 5*, N35Q/N62Q/N75QhPAR$_1$E; *lane 6*, N250Q/N259QhPAR$_1$E; *lane 7*, N35–259QhPAR$_1$E. *B*, protein samples of hPAR$_1$E-transfected CHO (Pro5 and Lec2) cell lines were immunoprecipitated by HA.11 immunoprecipitation and were analyzed by SDS-PAGE (10% gel) and immunoblotted using a monoclonal HA.11 antibody. *Lane 1*, Pro5; *lane 2*, Pro5-PAR$_1$E; *lane 3*, Lec2; *lane 4*, Lec2-PAR$_1$E. *GD*, glycosylated dimer; *NGD*, nonglycosylated dimer; *GM*, glycosylated monomer; *NGM*, nonglycosylated or minimally glycosylated monomer; *M*, nonglycosylated or minimally glycosylated monomer; *D*, PAR$_1$ dimer; *M.M.*, molecular mass. Results are representative of three separate experiments.

N62Q/N75QhPAR$_1$E migrated from ~37 to ~120 kDa. N35Q/N62Q/N75QhPAR$_1$E migrated with a molecular mass from ~37 to ~200 kDa, with the majority of the receptor being observed from ~75 to ~120 kDa. The predicted molecular mass of the fused hPAR$_1$eYFP is approximately ~70 to ~80 kDa (hPAR$_1$ is ~47 kDa, and eYFP protein is ~31 kDa). We proposed that the band at ~75 kDa may represent an unglycosylated monomer of PAR$_1$; the bands around ~80 to ~130 kDa may represent a glycosylated monomer of PAR$_1$; and the bands around ~150 to ~220 kDa may represent glycosylated and unglycosylated dimers of PAR$_1$ (Fig. 4). When removing all three glycosylation sites (Asn^{35}, Asn^{62}, and Asn^{75}) in the N terminus of the receptor, the banding pattern changed, with only glycosylated dimer and unglycosylated monomer present. Removal of glycosylation at sites Asn^{62} and Asn^{75} produced a single band at ~120 kDa representing a glycosylated monomer of PAR$_1$. Only one band migrated at ~37 kDa from both N250Q/N259QhPAR$_1$E and N35–259QhPAR$_1$E. A number of minor bands that may represent either eYFP protein or proteolytic degradation products of hPAR$_1$ were routinely observed around ~37 kDa in all lanes.

TABLE 2

EC$_{50}$ values for N-terminal glycosylation-deficient mutant hPAR$_1$ and their respective matching cell surface expression of WT hPAR$_1$ agonist concentration effect curves

Cell clones with matched receptor expression assessed by FACS analysis were selected for functional studies. Where it was not possible to match receptor expression between the WT hPAR$_1$ cell line and a cell line expressing a mutant glycosylation receptor, the WT, WT-H, WT-M, and WT-L with different cell confluence in order to reduce receptor expression were used and thus match the cell surface expression of the mutant cell line. Reduced receptor cell surface expression of the WT-H, WT-M, and WT-L cell lines were confirmed by using FACS analysis.

Cell lines with matched receptor expression	EC$_{50}$		
	TFLLR	Thrombin	Trypsin
	μM	nM	nM
WT-H	17	0.14	33
N35Q	16	0.2	43
WT-L	27	0.2	39
N62Q	29	0.4	43
N75Q	31	0.2	41
WT-M	22	0.12	26
N62Q/N75Q	30	0.3	42

To determine the contribution of sialic acid to the molecular mass of hPAR$_1$, we performed Western blot analysis for WT hPAR$_1$E-transfected CHO cells (Pro5 and Lec2) (Fig. 4*B*). No bands were detected in the non-transfected Lec2 and Pro5. Pro5-PAR$_1$E migrated as a broad high molecular weight band ranging from ~25 to ~200 kDa; the molecular mass of Lec2-PAR$_1$E ranged from ~25 to ~150 kDa. Two bands were routinely observed in the ~25 to ~37 kDa range in both Pro5-PAR$_1$E and Lec2-PAR$_1$E.

The N-Linked Glycosylation Located after the Tethered Ligand of hPAR$_1$ Regulates hPAR$_1$ Signaling—To investigate whether *N*-linked glycosylation at individual residues had a role in regulating receptor function, we constructed calcium signaling concentration-effect curves for thrombin, trypsin, and TFLLR-NH$_2$ in WT hPAR$_1$ and hPAR$_1$ glycosylation mutant KNRK cell lines. The EC$_{50}$ values of WT hPAR$_1$ and mutant receptors for the calcium signaling assay are displayed in Table 2.

N62Q/N75Q concentration effect curves were compared with WT-M because they displayed similar cell surface expression ($p > 0.05$) (Fig. 5*A*). TFLLR-NH$_2$ displayed a slight rightward shift in activating N62Q/N75Q compared with WT-M, stimulating a calcium signal at 3–100 μM for WT-M and 10–100 μM for N62Q/N75Q, respectively, but achieved the same maximum response of 42 ± 1.5% of A23187 at 100 μM in both cell lines (Fig. 5*B*). For N62Q/N75Q and WT-M, thrombin induced a calcium signal from 0.05 to 5 nM (Fig. 5*C*). However, the magnitude of the responses to thrombin in N62Q/N75Q was smaller than those obtained for WT-M (24 ± 2.6% of A23187 and 31 ± 1.8% of A23187, respectively) ($p > 0.05$). The EC$_{50}$ value for thrombin in N62Q/N75Q was 0.3 nM, and the EC$_{50}$ value in WT-M was 0.12 nM. Interestingly, the N62Q/N75Q displayed reduced sensitivity toward trypsin compared with WT-M, and the maximal response achieved was only 14% of A23187 compared with 32 ± 3% of A23187 for the WT-M ($p < 0.001$) (Fig. 5*D*). In addition, the EC$_{50}$ value for trypsin in N62Q/N75Q was significantly greater than WT-M (42 and 26 nM, respectively). However, further analysis of N62Q and N75Q

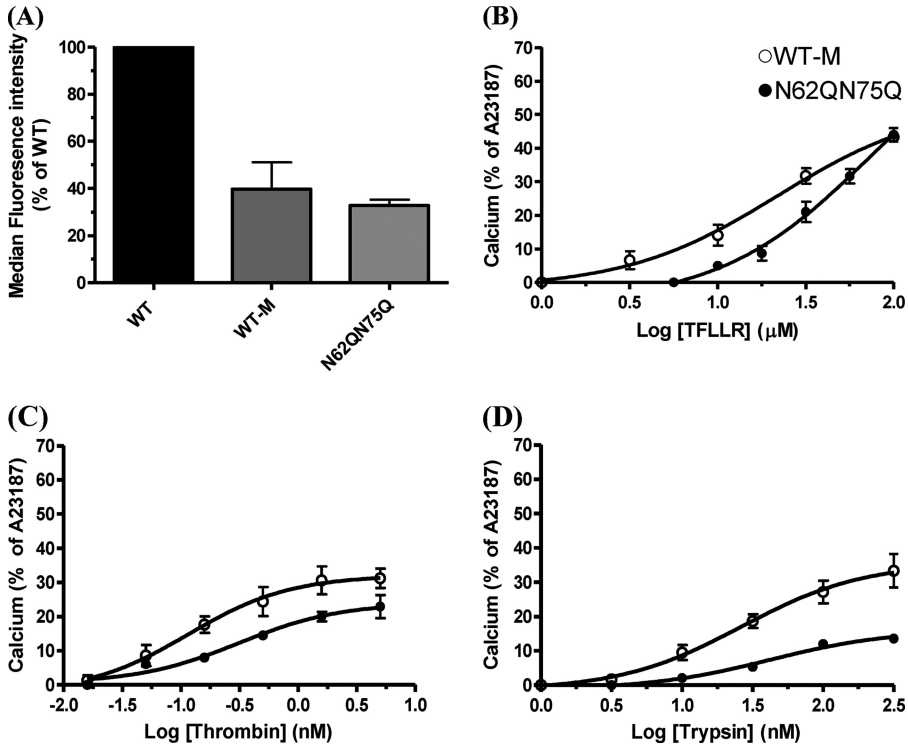

FIGURE 5. **Cell surface expression and calcium signaling analysis of WT-M and N62Q/N75Q.** *A*, comparison of WT-M and glycosylation-deficient mutant N62Q/N75Q KNRK cell surface expression. Cells at ~90% confluence were harvested and incubated with the ATAP-2 antibody before incubation with an anti-mouse FITC-conjugated antibody. Cell surface expression was assessed by FACS analysis. Results are expressed as a percentage of the median fluorescence obtained with WT cells. *B–D*, calcium signaling in the WT-M and glycosylation mutant N62Q/N75Q in response to TFLLR-NH$_2$, thrombin, and trypsin. Results are expressed as the means ± S.E. of at least four independent experiments.

cell lines revealed no observable changes in receptor function for TFLLR-NH$_2$, thrombin, or trypsin when compared with their matched WT hPAR$_1$ cell line (data not shown).

Removal of N-Linked Glycosylation Asn^{62} and/or Asn^{75} from hPAR$_1$ Enhances the Ability of Trypsin to Disarm the Receptor—Having found that trypsin shows reduced activity toward N62Q/N75Q by a calcium signaling assay, we then explored the ability of trypsin to disarm N62Q/N75Q, N62Q, and N75Q.

Fig. 6*A* shows the TFLLR-NH$_2$ (100 μM) responses following trypsin (3, 10, 30, 100, and 300 nM) and then thrombin (5 nM) challenge in WT-M and N62Q/N75Q cells (*i.e.* trypsin and then thrombin and then TFLLR-NH$_2$). For WT-M, the TFLLR-NH$_2$ responses remained the same after challenging the cells with trypsin from 3 to 300 nM. Challenging the N62Q/N75Q cells with 3 nM trypsin followed by 5 nM thrombin and then 100 μM TFLLR-NH$_2$ triggered a calcium signal that was similar to that seen for WT-M cells. However, a robust increase in the magnitude of TFLLR-NH$_2$-triggered calcium signal was observed after challenging the N62Q/N75Q cells with 300 nM trypsin, which was over 4-fold greater than that observed for WT-M cells ($p < 0.05$).

We next assessed whether individual glycosylation at Asn^{62} or Asn^{75} is responsible for regulating trypsin disarming of hPAR$_1$ (Fig. 6, *B* and *C*). Challenging N62Q cells with 5 nM thrombin or 100 μM TFLLR-NH$_2$ resulted in a calcium response of 61.4 ± 6.7% of A23187 and 62 ± 6.9% of A23187, respectively (Fig. 6*B*). Challenging N62Q cells with 100 nM trypsin resulted in an observable calcium signal (32 ± 8% of A23187). The addition of thrombin following trypsin challenge resulted in a marked reduction ($p < 0.001$) in the calcium response to thrombin compared with the response obtained with thrombin added alone (7.8 ± 1% of A23187 *versus* 61.4 ± 6.7% of A23187). The addition of TFLLR-NH$_2$ following trypsin and thrombin resulted in a response that was slightly increased ($p > 0.05$) in magnitude compared with the response obtained to TFLLR-NH$_2$ following just thrombin addition (17.5 ± 3.6% of A23187 *versus* 9 ± 3% of A23187) but was significantly reduced ($p < 0.001$) compared with the response of TFLLR-NH$_2$ added alone (17.5 ± 3.6% of A23187 *versus* 62 ± 6.9% of A23187).

Challenging N75Q cells with trypsin only resulted in a response of 8 ± 1% of A23187 (Fig. 6*C*). Challenging N75Q cells with TFLLR-NH$_2$ or thrombin alone resulted in a calcium response of 27 ± 2% of A23187 and 12 ± 0.7% of A23187, respectively. The addition of TFLLR-NH$_2$ following thrombin addition resulted in a calcium response of 12 ± 1.7% of A23187. The addition of thrombin following the addition of trypsin resulted in no calcium response. Finally, challenging the cells with TFLLR-NH$_2$ following trypsin and thrombin addition triggered a calcium response of 21 ± 2.7% of A23187, which was of a magnitude comparable ($p > 0.05$) with the response obtained with TFLLR-NH$_2$ alone.

Elastase, Proteinase 3, and Thermolysin but Not Cathepsin G Displayed Enhanced Ability to Disarm hPAR$_1$(N62Q/N75Q)—Effective proteinase receptor disarming was assessed by thrombin activation of the cells following proteinase addition. For N62Q/N75Q and WT-M, significant differences ($p < 0.0001$) in responses to 5 nM thrombin following the addition of elastase

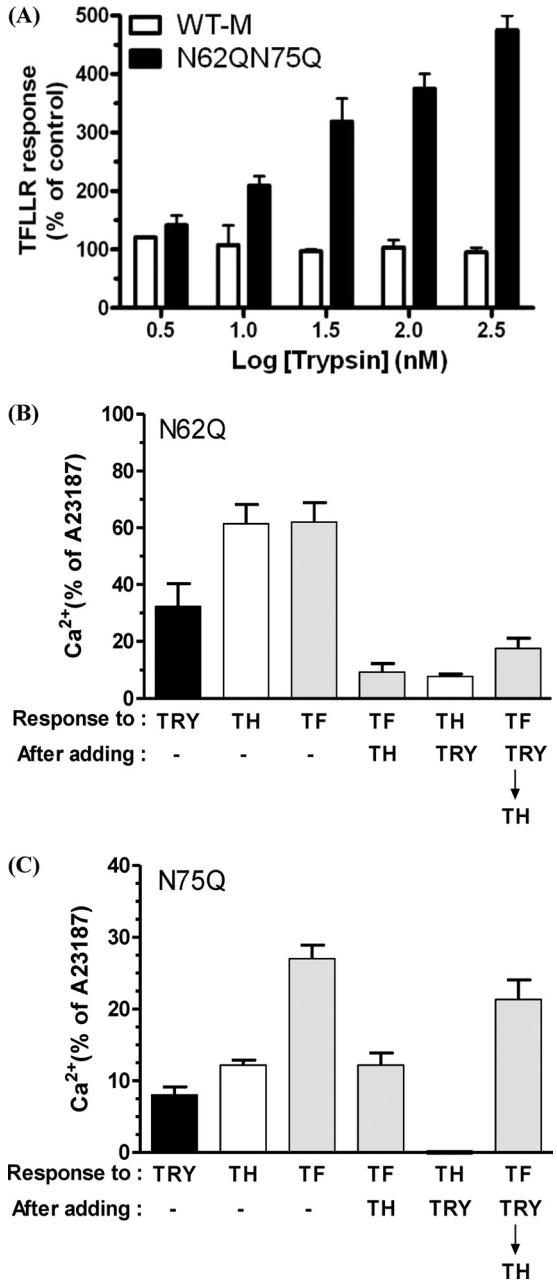

FIGURE 6. *A*, analysis of trypsin disarming in WT-M and N62Q/N75Q. Calcium imaging of Fluo-3-loaded cells was used to assess 100 μM TFLLR-NH$_2$ responses following trypsin and then 5 nM thrombin challenge in WT hPAR$_1$- and hPAR$_1$(N62Q/N75Q)-transfected KNRK cells. The cellular response to TFLLR-NH$_2$ after the addition of thrombin but without pretreatment with trypsin is used as a percentage control. *B*, analysis of trypsin disarming in N62Q. Shown is hPAR$_1$(N62Q)-transfected KNRK cell calcium signaling response following the addition of 100 nM trypsin, 5 nM thrombin, and 100 μM TFLLR-NH$_2$ and then 2 μM A23187. *C*, analysis of trypsin disarming in N75Q. Shown is hPAR$_1$(N75Q)-transfected KNRK cell calcium signaling response following the addition of 100 nM trypsin, 5 nM thrombin, 100 μM TFLLR-NH$_2$, and then 2 μM A23187. *TRY*, trypsin; *TH*, thrombin; *TF*, TFLLR-NH$_2$. The data sets are expressed as mean ± S.E. (*error bars*) from three separate experiments.

at different concentrations were observed (Fig. 7*A*). For WT-M, no changes were observed in thrombin-triggered calcium responses after the addition of 1 nM elastase, and the thrombin-triggered calcium response was totally ablated after the addition of 15 nM elastase. The thrombin response curve for N62Q/N75Q shifted left half a log when compared with WT-M. For N62Q/N75Q, the calcium signaling response to thrombin started to decrease after challenging the cells with 1 nM elastase (~80% of control thrombin response). The thrombin-triggered calcium response was totally ablated after challenging cells with 5 nM elastase.

For N62Q/N75Q and WT-M, no significant differences ($p > 0.05$) in responses to 5 nM thrombin following the addition of cathepsin G from 10 to 300 nM were observed (Fig. 7*B*). The thrombin-triggered calcium response was totally ablated after the addition of 300 nM cathepsin G for both N62Q/N75Q and WT-M.

For N62Q/N75Q and WT-M, significant differences ($p < 0.0001$) in responses to 5 nM thrombin following the addition of proteinase 3 were observed (Fig. 7*C*). For WT-M, no changes were observed in the thrombin-triggered calcium response following the addition of 1000 nM proteinase 3. In contrast, significant decreases in the response to thrombin were observed in N62Q/N75Q following the addition of proteinase 3 from 1 to 1000 nM. The thrombin-triggered calcium signal was totally abolished after the addition of 1000 nM proteinase 3.

For N62Q/N75Q and WT-M, significant differences ($p < 0.0001$) in responses to 5 nM thrombin following the addition of thermolysin at different concentrations were observed (Fig. 7*D*). The thrombin response curve after adding thermolysin at increasing concentration for N62Q/N75Q shifted 30-fold to the left when compared with WT-M. For N62Q/N75Q, the calcium signaling response to thrombin started to decrease after application of thermolysin at 3 nM (~80% of control thrombin response). The thrombin-triggered calcium response was totally ablated after challenging N62Q/N75Q with 300 nM thermolysin. However, for WT-M, the thrombin-triggered calcium responses remained elevated at thermolysin concentrations up to 30 nM. The calcium signaling response to thrombin started to decrease following the 100 nM thermolysin addition (~80% of thrombin control). The thrombin-triggered calcium response in WT-M was totally ablated after the addition of 1000 nM thermolysin.

Molecular Evidence That Cathepsin G and Proteinase 3 Are Disarming hPAR$_1$(N62Q/N75Q)—The addition of 100 nM cathepsin G to N62Q/N75Q cells before the addition of 5 nM thrombin markedly reduced ($p < 0.001$) the response to thrombin compared with the response obtained with thrombin added alone (11 ± 2% of A23187 and 30 ± 5% of A23187, respectively) (Fig. 8*A*). In contrast, the prior addition of cathepsin G failed to reduce the thrombin calcium signal in cathepsin G mutant cells when compared with the control (32.5 ± 8% of A23187 and 36.5 ± 8% of A23187, respectively) ($p > 0.05$).

No observable calcium response to thrombin was observed when 300 nM proteinase 3 had been added to the N62Q/N75Q cells prior to thrombin challenge (Fig. 8*B*). In contrast, the prior addition of proteinase 3 failed to reduce the thrombin calcium signal in the proteinase 3 mutant cells, when compared with the response obtained with thrombin added alone (13 ± 2% of A23187 and 12.33 ± 2.5% of A23187, respectively) ($p > 0.05$).

Elastase, Cathepsin G, Proteinase 3, and Thermolysin Mainly Disarm hPAR$_1$(N75Q)—The ability of thermolysin and neutrophil serine proteinases to activate/disarm N62Q and N75Q was investigated (Fig. 9).

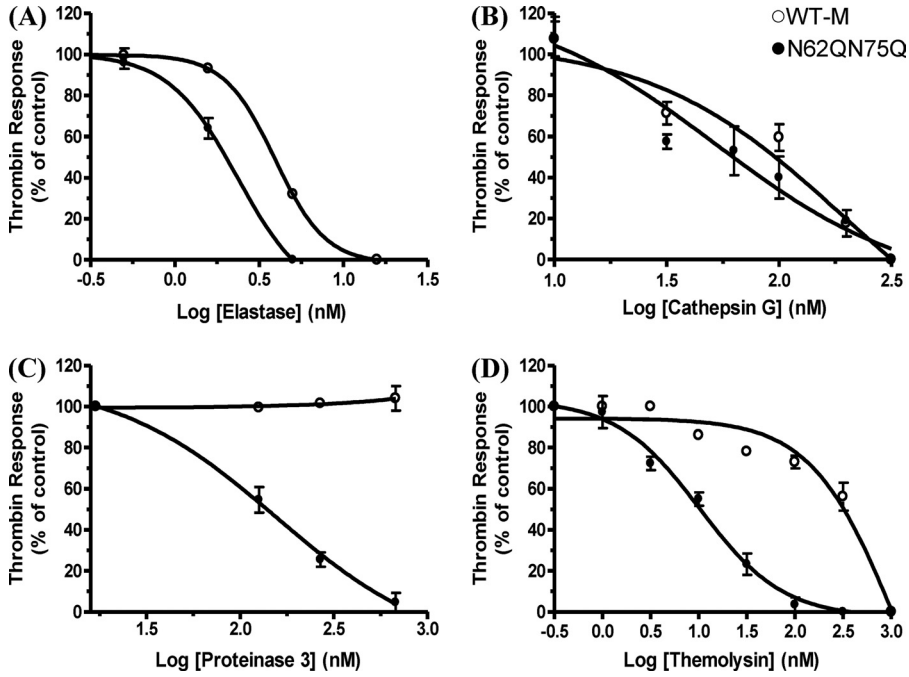

FIGURE 7. **Analysis of WT-M and hPAR$_1$(N62Q/N75Q) calcium signaling following proteinase stimuli.** WT-M and N62Q/N75Q in KNRK cells were challenged by the addition of elastase (*A*), the addition of cathepsin G (*B*), the addition of proteinase 3 (*C*), or the addition of thermolysin (*D*) followed by the addition of 5 nM thrombin and finally the addition of 2 μM A23187. Results are expressed as mean ± S.E. from at least three independent experiments.

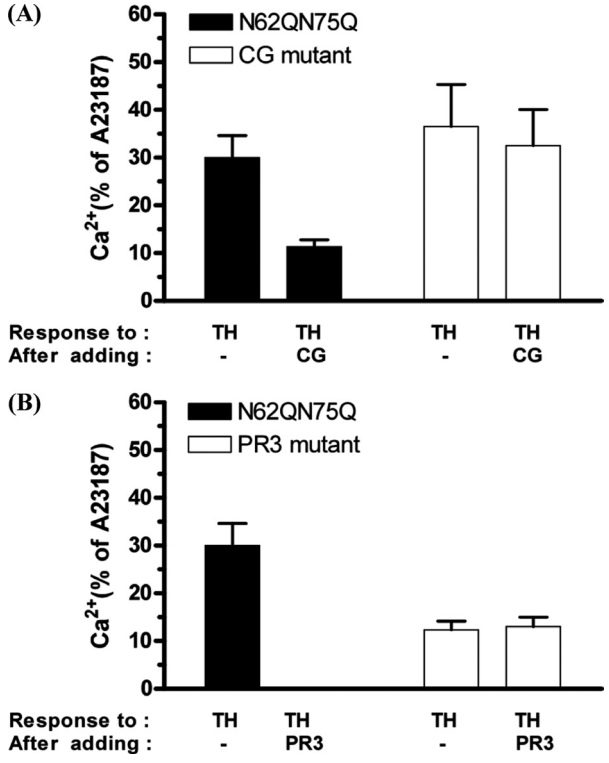

FIGURE 8. **Molecular evidence that cathepsin G and proteinase 3 disarm hPAR$_1$(N62Q/N75Q).** CG mutant (*A*) and proteinase 3 mutant (*B*) cells loaded with Fluo-3 were stimulated by the addition of either 100 nM cathepsin G or 300 nM proteinase 3 for 2 min and then challenged with 5 nM thrombin, followed by 100 μM TFLLR-NH$_2$ and then 2 μM calcium ionophore (A23187). *TH*, thrombin; *CG*, cathepsin G; *PR3*, proteinase 3. Results are expressed as the mean ± S.E. (*error bars*) of at least two independent experiments.

Challenging N62Q cells with 5 nM thrombin or 100 μM TFLLR-NH$_2$ resulted in a calcium response of 64.7 ± 7% of A23187 and 67.8 ± 5% of A23187, respectively (Fig. 9*A*). In addition, challenge with TFLLR-NH$_2$ following the thrombin addition resulted in a calcium response of 9 ± 3% of A23187. Thermolysin (50 nM) had no observable effect on calcium signaling in N62Q. Challenge with thrombin following the thermolysin addition resulted in a calcium response at 53.5 ± 4.6% of A23187, which is comparable with that obtained with thrombin added alone (64.7 ± 7% of A23187). The addition of TFLLR-NH$_2$ following thermolysin and thrombin resulted in a similar calcium response to the response obtained with TFLLR-NH$_2$ following just thrombin challenge (13.6 ± 4% of A23187 and 9 ± 3% of A23187, respectively). The addition of 1.5 nM elastase had no observable effect on calcium signaling in N62Q cells. The addition of thrombin following elastase addition resulted in a calcium response of 49 ± 3.5% of A23187. The addition of TFLLR-NH$_2$ following the disarming with elastase and thrombin resulted in a similar calcium response to the TFLLR-NH$_2$ response obtained following just thrombin alone 12 ± 1% of A23187 and 9 ± 3% of A23187, respectively). The addition of 100 nM cathepsin G had no observable effect on calcium signaling in N62Q cells. After challenging N62Q cells with cathepsin G, the addition of thrombin resulted in a small decrease in the calcium response compared with that obtained with thrombin added alone (39 ± 3.8% of A23187 and 64.7 ± 7% of A23187, respectively). The addition of TFLLR-NH$_2$ following the addition of thermolysin and thrombin triggered a calcium response at 16 ± 6% of A23187 that was slightly larger than that obtained with TFLLR-NH$_2$ following thrombin alone (9 ± 3% of A23187). The addition of 300 nM proteinase 3 had no observable effect on calcium signaling in N62Q cells. Challenge with thrombin following proteinase 3 addition resulted in a calcium response of 67 ± 6.7% of A23187, which is comparable with that obtained when thrombin was added alone (64.7 ± 7% of A23187). The addition of TFLLR-NH$_2$ following the addition of

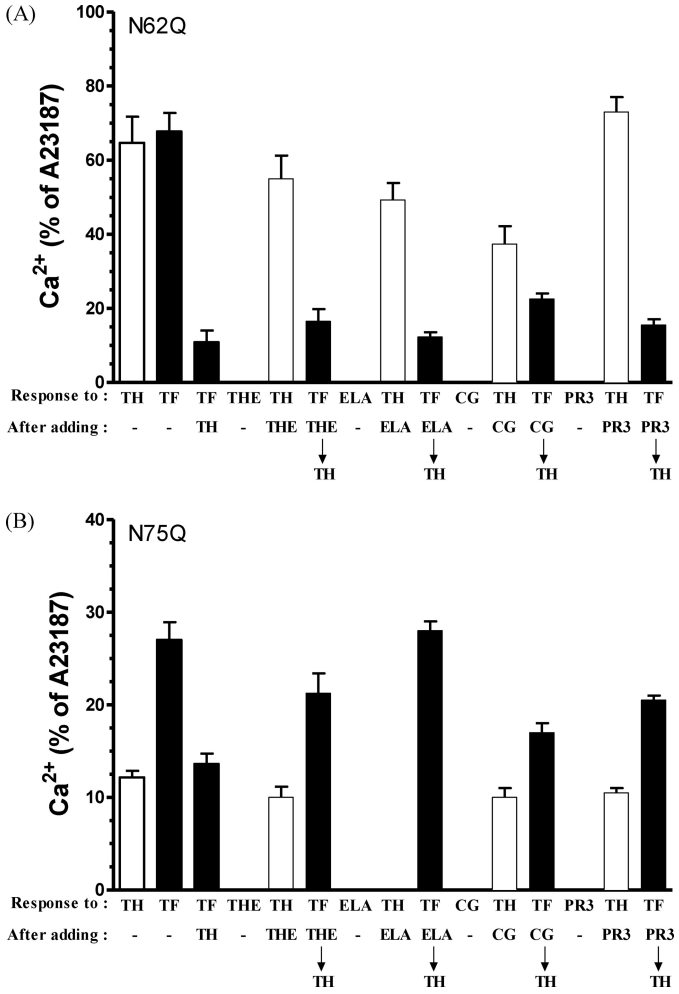

FIGURE 9. **Analysis of hPAR$_1$(N62Q) and hPAR$_1$(N75Q) calcium signaling following proteinase stimuli.** N62Q (*A*) and N75Q (*B*) cells loaded with Fluo-3 were stimulated by the addition of either 50 nM thermolysin, 1.5 nM elastase, 100 nM cathepsin G, or 300 nM proteinase 3 for 2 min and then challenged with 5 nM thrombin, followed by 100 μM TFLLR-NH$_2$ and then 2 μM A23187. *TRY*, trypsin; *TH*, thrombin; *TF*, TFLLR-NH$_2$; *THE*, thermolysin; *ELA*, elastase; *CG*, cathepsin G; *PR3*, proteinase 3. Results are expressed as the mean ± S.E. (*error bars*) of at least three independent experiments.

proteinase 3 and thrombin resulted in a calcium response similar to that obtained with TFLLR-NH$_2$ following the thrombin addition (11.6 ± 4% of A23187 and 9 ± 3% of A23187, respectively).

Challenging N75Q cells with thrombin or TFLLR-NH$_2$ resulted in a calcium response of 12 ± 0.7% of A23187 and 27 ± 2% of A23187, respectively. The addition of TFLLR-NH$_2$ following thrombin challenge resulted in a calcium response of 13.6 ± 1% of A23187 (Fig. 9*B*). No observable calcium response was detected after challenging N75Q cells with thermolysin. After challenging N75Q cells with thermolysin, the addition of thrombin resulted in a calcium response that was comparable with that obtained to thrombin alone (10 ± 1% of A23187 and 12 ± 0.7% of A23187, respectively), and finally challenging the cells with TFLLR-NH$_2$ triggered a calcium response of 21 ± 2% of A23187. No observable calcium response was detected after challenging N75Q cells with elastase or with thrombin following the addition of elastase. In addition, the response to TFLLR-NH$_2$ following elastase and thrombin challenge was the same as that obtained with TFLLR-NH$_2$ alone (28 ± 1% of A23187 *versus* 27 ± 2% of A23187).

The addition of cathepsin G had no observable effect on calcium signaling in N75Q cells. Challenging cells with thrombin following the addition of cathepsin G resulted in a calcium response of 10 ± 1% of A23187, which was comparable with that obtained with thrombin alone (12 ± 0.7% of A23187). The addition of TFLLR-NH$_2$ following the addition of cathepsin G and thrombin triggered a calcium response, which was of a magnitude similar to that obtained with TFLLR-NH$_2$ following thrombin alone (17 ± 1 and 13.6 ± 1% of A23187, respectively). The addition of proteinase 3 had no observable effect on calcium signaling in N75Q cells. The addition of thrombin after challenging N75Q cells with proteinase 3 resulted in a very small decrease in calcium response compared with that obtained with thrombin alone (10 ± 0.5% of A23187 and 12 ± 0.7% of A23187, respectively). Finally, challenging the cells with TFLLR-NH$_2$ following the proteinase 3 and thrombin addition triggered a calcium response of 20.5 ± 0.5% of A23187.

DISCUSSION

In the present study, we have demonstrated for the first time that *N*-linked glycans (Asn^{62} and Asn^{75}) after the tethered ligand on the N terminus of hPAR$_1$ regulate receptor signaling to trypsin, thermolysin, and the neutrophil proteinases elastase and proteinase 3 but not cathepsin G. In addition, we reported that hPAR$_1$ is heavily *N*-linked glycosylated and sialylated in epithelial cell lines (KNRK and Pro5 cells), and glycosylation occurs at all five consensus sites, namely Asn^{35}, Asn^{62}, Asn^{75}, Asn^{250}, and Asn^{259}. Removing *N*-linked glycosylation sequons at these positions affected hPAR$_1$ cell surface expression to varying degrees, and *N*-linked glycosylation at ECL2 (especially Asn^{250}) of hPAR$_1$ might be essential for optimal receptor cell surface expression and receptor stability.

N-Linked glycosylation, which adds oligosaccharides to the nitrogen in the side-chain amide of asparagine residues, requires the asparagines in a consensus sequence of Asn-*X*-Ser/Thr (where *X* is any amino acid except proline) (22, 23). However, not all consensus sites are actually glycosylated because the oligosaccharide might be trimmed and elaborated during transit through the endoplasmic reticulum and the Golgi apparatus (23). Disrupting the glycosylation sites by mutagenesis, individually and/or in combination, allowed us to investigate the status and even the function of each specific putative *N*-linked glycosylation site.

We first examined the role of *N*-linked glycosylation in regulating the receptor cell surface expression and the receptor global distribution in KNRK cells. Interestingly, unlike in previous studies in HeLa (24), there is still a very high level of cell surface expression of hPAR$_1$ when removing all glycosylation sites on the N terminus. The ECL2 single glycosylation mutant N250Q displayed the lowest level of cell surface expression of hPAR$_1$ among all of the other single glycosylation mutants; furthermore, removing all glycosylation sequons on ECL2 resulted in similar low levels of receptor cell surface expression to the non-glycosylation mutant, where all glycosylation sequons had been deleted. *N*-Linked glycosylation of hPAR$_1$ on ECL2 (especially Asn^{250}) *versus* glycosylation in the N terminus might

therefore be more important for receptor optimal cell surface expression. Glycosylation on ECL2 of PAR_2 is also important for enhancing receptor expression but not regulating receptor signaling; more importantly, the ECL2 region is extremely sensitive to mutations, and mutating residues in and around the glycosylation sequon, even neutral mutations such as alanine (Ala) in the ECL2 glycosylation sequon, alters receptor structure and function (19, 24). The PAR_1 glycosylation study on HeLa cells (24) reported that N-terminal *N*-linked glycosylation of PAR_1 *versus* ECL2 *N*-linked glycosylation is critical for the regulation of PAR_1 signaling and trafficking. In this study, mutants were generated by substituting Ala for Glu. It is therefore hard to determine whether the altered $hPAR_1$ cell surface expression and signaling in HeLa cells are a result of the loss of *N*-linked glycosylation or due to the Ala substitution altering receptor structure and function. We have generated our *N*-linked glycosylation mutants by substituting Asn for Glu at all five potential *N*-linked glycosylation sites; Glu is chemically and structurally more similar to Asn. For this reason, we propose that this substitution itself will not lead to structural and functional differences between the mutants and wild-type $hPAR_1$, and any differences detected should be due to the loss of glycosylation.

Using confocal microscopy, we demonstrated that the glycosylation-deficient mutants were abundant in the cytosol. Removal of a single N-terminal glycan resulted in observable receptor cytosolic retention, but removal of all glycosylation sites produced a receptor that could mainly be seen in the cytosol with minimal cell surface expression. Therefore, we conclude that *N*-linked glycosylation of $hPAR_1$ at all sites might be required for the optimal receptor cell surface expression (24, 25).

Similar to the study of Soto and Trejo (24), we have demonstrated that in KNRK cells, $hPAR_1$ is heavily glycosylated, and the glycosylation occurs at all five consensus sites. Removal of *N*-linked glycosylation from ECL2 or removal of all *N*-linked glycans from the receptor resulted in only a single Western blot band visualized at around 37 kDa compared with wild type or the N terminus mutants, which produced a second band at a lower molecular weight. It is well known that *N*-linked glycosylation can regulate receptor conformation, folding, or stability and even protect receptors from proteolytic degradation. The bands shown around ~37 kDa may represent either eYFP protein or deglycosylation and/or proteolytic degradation products of $hPAR_1$ (5, 14, 24, 26–28). We thus propose that *N*-linked glycosylation, especially on ECL2 (Asn^{250} and Asn^{259}), of $hPAR_1$ might be vital for receptor stability and even protect $hPAR_1$ from endogenous proteolytic degradation. Furthermore, we expressed the $hPAR_1$ in CHO cells (Pro5 and Lec2) in order to assess the sialylation status of $hPAR_1$. The Pro5 cell line is the parent clone for the Lec2 cell line, which has a substantial loss in the ability to attach sialic acid to the terminal positions on oligosaccharides. Western blot analysis of $hPAR_1$ in Lec2 cells revealed a protein that had a molecular mass that was up to ~47 kDa lower than that observed for $hPAR_1$ expressed in the Pro5 cells. Presumably, this significant loss of ~47 kDa is due to the loss of receptor-associated sialic acid, and we can therefore conclude that $hPAR_1$ in Pro5 cells, at least, is a heavily sialylated receptor.

In order to establish the role of *N*-linked glycosylation on the N terminus of $hPAR_1$ in regulating receptor function, agonist concentration effect curves were produced for the glycosylation-deficient $hPAR_1$ cell lines and their respective WT $hPAR_1$ cell line to evaluate the coupling of the mutant receptors to calcium. Receptor cell surface expression for each mutant cell line was compared and matched by FACS to WT $hPAR_1$ cells in order to ensure that any functional differences detected were not due to differences in receptor cell surface expression (19). Except for the N62Q/N75Q mutant, no significant changes in receptor function were detected when compared with their respective matching WT $hPAR_1$ for all mutant cell lines. This N62Q/N75Q mutant displayed a slight reduction in sensitivity toward lower concentrations of TFLLR-NH_2 and thrombin, although statistical analysis showed no significant differences in EC_{50} value and receptor maximum calcium signaling response toward 100 μM TFLLR-NH_2 or 5 nM thrombin. The biggest reduction in agonist sensitivity was observed with trypsin activation. PAR_1 coupling to calcium signaling appears not to be affected by the lack of glycosylation on the receptor. Even the N35–259Q mutant cell line still displayed a detectable calcium signal toward TFLLR-NH_2 and thrombin (data not shown), thus adding strength to this conclusion.

In our experiments, trypsin triggered calcium signaling in wild-type $hPAR_1$ and its mutants to varying degrees. However, the TFLLR-NH_2 calcium signaling response after the addition of trypsin and thrombin is much greater in N62Q/N75Q mutants compared with wild-type $hPAR_1$. This just confirmed that trypsin disarms the mutant receptor, and the disarmed mutant receptors still remained on the cell surface but could not be activated by thrombin anymore because the tethered ligand had been removed; however, TFLLR will still activate those mutant receptors by binding to receptor ECL2. Trypsin can activate PAR_1 by cleaving at the activating cleavage site Arg^{41}-Ser^{42} to expose the tethered ligand (2, 4, 29). Moreover, trypsin has also been reported to cleave PAR_1 at residues Arg^{70}-Leu^{71} and Lys^{82}-Gln^{83}, which amputates the tethered ligand from the receptor (4) (Fig. 1). Furthermore, these residues are suggested to be cleaved by trypsin much faster than the residues Arg^{41}-Ser^{42} (9). Given that these two potential trypsin cleavage sites are located close to Asn^{75}, it is not surprising that in the N62Q/N75Q and N75Q mutants, trypsin can gain easy access to these cleavage sites and therefore disarm these mutant receptors. In contrast, when PAR_1 is fully glycosylated at Asn^{75}, these cleavage sites are subsequently shielded by the attached oligosaccharide, and thus trypsin disarms WT $hPAR_1$ less efficiently. Interestingly, the previous study by Nakayama *et al.* (9) reported that 100 nM trypsin cleaved PAR_1 but did not activate it in HUVEC cells, thus suggesting receptor disarming. We therefore assume that the glycosylation status of PAR_1 in HUVEC cells must be different from our PAR_1-KNRK system. Indeed, previous studies reported that PAR_1 expressed in HUVECs and platelets migrated as a homogenous species with an apparent mass of 66 kDa (27). This molecular mass is considerably below that reported in other cell systems, including ours, and suggests that PAR_1 is not so heavily glycosylated in

these cell types. Therefore, we suggest that the Asn^{62} and Asn^{75} might not be fully glycosylated in HUVECs, and therefore these potential trypsin cleavage sites around Asn^{75} are more readily available for trypsin cleavage and subsequent disarms.

We have also shown that the neutrophil proteinases elastase, cathepsin G, and proteinase 3 do not activate PAR$_1$ in our KNRK cell system but rather disarm the receptor. Like us, Renesto *et al.* (13) reported that elastase, cathepsin G, and proteinase 3 can cleave and inactivate PAR$_1$ in platelets and human endothelial cells. In contrast, Suzuki *et al.* (8) reported that elastase can activate PAR$_1$ in human lung epithelial cells and also mentioned that proteolytic cleavage of PAR$_1$ by elastase might activate or inactivate the receptor depending on the site of cleavage. The authors also suggested that the extent of glycosylation of the receptor could influence the site and extent of cleavage of the receptor (8).

In our current study, we note that elastase disarms N62Q/N75Q better than WT hPAR$_1$ at the same concentration, and 1.5 nM elastase disarms N75Q, but not N62Q. The mass spectrometry study by Renesto *et al.* (13) indicated that elastase cleaves the N terminus of hPAR$_1$ at Val^{72}-Ser^{73} and Ile^{74}-Asn^{75}, which are located after the tethered ligand. Furthermore, Loew *et al.* (4) reported that elastase cleaved the PAR$_1$ exodomain at Ala^{36}-Thr^{37}, Val^{72}-Ser^{73}, and Ala^{86}-Phe^{87} sites with preferential cleavage at Val^{72}, which would disable the receptor. Therefore, after amputating the Asn^{75} glycosylation, the potential cleavage sites Val^{72}-Ser^{73} might be more easily accessible for elastase cleavage.

Because cathepsin G has been reported to have both activating and disarming actions on PARs (12, 13, 30, 31), we tested the role of N-terminal glycosylation of hPAR$_1$ in regulating this proteinase. We have demonstrated that cathepsin G could clearly disarm N62Q/N75Q and WT hPAR$_1$ to the same efficiency. In addition, our data also revealed that cathepsin G at 100 nM disarms N62Q and N75Q. Like us, others have also reported that cathepsin G at 30 nM could disarm PAR$_1$ (30). Molino *et al.* (12) reported that in addition to the Arg^{41}-Ser^{42} site, cathepsin G cleaves PAR$_1$ at Phe^{43}-Leu^{44} and Phe^{55}-Trp^{56}, removing the tethered ligand and rendering the receptor unresponsive to thrombin. In 1997, the mass spectrometry study of Renesto *et al.* (13) indicated that cathepsin G cleaves PAR$_1$ on platelets and endothelial cells downstream of the thrombin cleavage site at Phe^{55}-Trp^{56} and Tyr^{69}-Arg^{70}. Thus, we then concluded that cathepsin G might have four potential cleavage sites in the N terminus of hPAR$_1$ (Arg^{41}-Ser^{42}, Phe^{43}-Leu^{44}, Phe^{55}-Trp^{56}, and Tyr^{69}-Arg^{70}). Furthermore, the kinetic analyses of Loew *et al.* (4) showed that the preferential cathepsin G cleavage site for PAR$_1$ is the Phe^{55}-Trp^{56} site. Moreover, our finding with the cathepsin G mutant is in accord with a previous report that has demonstrated that Phe^{55}-Trp^{56} is the main region cleaved within the receptor N terminus by cathepsin G (12). Also, our Western blot data revealed that Asn^{62} is not heavily glycosylated in our KNRK system. Therefore, we suggest that cathepsin G sensitivity toward hPAR$_1$ is not regulated by *N*-linked glycosylation.

We have also assessed proteinase 3 inhibition of thrombin-induced Ca^{2+} mobilization in WT hPAR$_1$, N62Q/N75Q, N62Q, and N75Q. Our data revealed that 300 nM proteinase 3 disarms N62Q/N75Q but not WT hPAR$_1$, N62Q, or N75Q. It is well established that proteinase 3 has an elastase-like specificity for Ala, Ser, and Val at the P1 site (32). One previous study on human oral epithelial cells (33) also pointed out that proteinase 3 can rapidly cleave PAR$_2$ between Arg and Ser and relatively inefficiently cleave between Lys and Val. Furthermore, proteinase 3 cleaved the peptide corresponding to the N terminus of PAR$_2$ at Arg^{36}-Ser^{37}, indicating that the site of the PAR$_2$ is structurally accessible by proteinase 3 (33). Interestingly, one previous study on synthetic peptides (13) reported that the cleavage site for proteinase 3 in the N terminus of PAR$_1$ is Val^{72}-Ser^{73}. In addition, the kinetic analysis of Loew *et al.* (4) on the N terminus domain of PAR$_1$ showed that proteinase 3 early cleavage sites for PAR$_1$ are Ala^{36}-Thr^{37}, Pro^{48}-Asn^{49}, Val^{72}-Ser^{73}, and Ala^{92}-Ser^{93}, and the late cleavage site is Pro^{54}-Phe^{55}. Furthermore, Sokolova and Reiser (29) suggested in a recent review that proteinase 3 cleaves human PAR$_1$ at Ala^{36}-Thr^{37} and Val^{72}-Ser^{73}. Although there are differences, previous studies have agreed that the Val^{72}-Ser^{73} might be the earliest cleavage site for proteinase 3. We therefore altered that site by creating a mutation, Ala^{72}-Ala^{73}, in our N62Q/N75Q (named the proteinase 3 mutant), and indeed the proteinase 3 almost immediately lost the ability to disarm the mutant receptor. As mentioned by Loew *et al.* (4), there exists a late cleavage site between Pro^{54} and Phe^{55}; we therefore suggest that apart from the Val^{72}-Ser^{73} cleavage site, there might exist relatively inefficient later cleavage events between Pro^{54} and Phe^{55} and possibly at Pro^{48}-Asn^{49}. Thus, there might be a possibility that if we expose PAR$_1$ to proteinase 3 for a greater length of time, proteinase 3 might disarm WT hPAR$_1$. Indeed, we did notice that this phenomenon happened when we preincubated PAR$_1$ with proteinase 3 for more than 3 min (data not shown). We have shown that in WT hPAR$_1$ cells, proteinase 3 does not disarm the receptor immediately (within 1 min); however, after the removal of the glycans in Asn^{62} and Asn^{75}, proteinase 3 immediately disarmed the glycosylation mutant receptor and inhibited thrombin-induced calcium mobilization. We therefore suggest that glycosylation of Asn^{62} and Asn^{75} together regulate hPAR$_1$ signaling to proteinase 3.

Our data also revealed that thermolysin disarms N62Q/N75Q with 30-fold better efficiency than WT hPAR$_1$. One previous study in insect SF9 cells (34) reported that thermolysin may represent an important mechanism of rapid receptor deactivation of the human thrombin receptor. Furthermore, like us, one previous study on PAR$_1$ in astrocytes (35) found that treatment with thermolysin generated a thrombin-insensitive receptor, whereas the response to the activating peptide was not affected. In the literature, it is well established that the predicted thermolysin cleavage sites in PAR$_1$ are within the tethered ligand domain (SFLLR) at Phe^{43}-Leu^{44} and Leu^{44}-Leu^{45}, suggesting that thermolysin would be expected to remove the exodomain of PAR$_1$ and destroy the tethered ligand and thus disarm the receptor (16, 36). Interestingly, in our study system, removing both of the glycosylation sequons (Asn^{62} and Asn^{75}) resulted in a receptor that was more efficiently disarmed by thermolysin, whereas removal of glycosylation at the Asn^{62} sequon alone from the receptor had no observable effect on thermolysin disarming. However, the N75Q did display

increased disarming compared with WT $hPAR_1$, thus suggesting that this sequon regulates PAR_1 disarming by thermolysin. Therefore, we predict that, apart from the well established cleavage sites, there might be some other thermolysin cleavage sites in the N terminus of PAR_1, especially in the region of the glycosylation site Asn^{75}. In theory, bacterial thermolysin cleaves peptide bonds N-terminally to the hydrophobic residues leucine and isoleucine, with some specificity for phenylalanine and valine (36). Therefore, we suggest that Leu^{71}-Val^{72} in PAR_1 may also be a potential thermolysin cleavage site, and it is very close to the Asn^{75} site. When amputating the Asn^{75} glycan, this potential thermolysin cleavage site (Leu^{71}-Val^{72}) will be more readily available for thermolysin cleavage.

In summary, $hPAR_1$ is a heavily glycosylated receptor and is important for cell surface expression, receptor stability, and function. We show here for the first time that glycosylation in the N terminus of $hPAR_1$ downstream of the tethered ligand (especially Asn^{75}) governs receptor disarming to trypsin, thermolysin, and the neutrophil proteinases elastase and proteinase 3 but not cathepsin G. Thus, we concluded that *N*-linked glycosylation at the N terminus of $hPAR_1$ plays a vital role in regulating the susceptibility to proteinase disarming of the receptor.

REFERENCES

1. Ramachandran, R., and Hollenberg, M. D. (2008) *Br. J. Pharmacol.* **153,** Suppl. 1, S263–S282
2. Macfarlane, S. R., Seatter, M. J., Kanke, T., Hunter, G. D., and Plevin, R. (2001) *Pharmacol. Rev.* **53,** 245–282
3. Hirano, K. (2007) *Arterioscler. Thromb. Vasc. Biol.* **27,** 27–36
4. Loew, D., Perrault, C., Morales, M., Moog, S., Ravanat, C., Schuhler, S., Arcone, R., Pietropaolo, C., Cazenave, J. P., van Dorsselaer, A., and Lanza, F. (2000) *Biochemistry* **39,** 10812–10822
5. Vouret-Craviari, V., Grall, D., Chambard, J. C., Rasmussen, U. B., Pouysségur, J., and Van Obberghen-Schilling, E. (1995) *J. Biol. Chem.* **270,** 8367–8372
6. Suidan, H. S., Bouvier, J., Schaerer, E., Stone, S. R., Monard, D., and Tschopp, J. (1994) *Proc. Natl. Acad. Sci. U.S.A.* **91,** 8112–8116
7. Molino, M., Barnathan, E. S., Numerof, R., Clark, J., Dreyer, M., Cumashi, A., Hoxie, J. A., Schechter, N., Woolkalis, M., and Brass, L. F. (1997) *J. Biol. Chem.* **272,** 4043–4049
8. Suzuki, T., Moraes, T. J., Vachon, E., Ginzberg, H. H., Huang, T. T., Matthay, M. A., Hollenberg, M. D., Marshall, J., McCulloch, C. A., Abreu, M. T., Chow, C. W., and Downey, G. P. (2005) *Am. J. Respir. Cell Mol. Biol.* **33,** 231–247
9. Nakayama, T., Hirano, K., Shintani, Y., Nishimura, J., Nakatsuka, A., Kuga, H., Takahashi, S., and Kanaide, H. (2003) *Br. J. Pharmacol.* **138,** 121–130
10. Schechter, N. M., Brass, L. F., Lavker, R. M., and Jensen, P. J. (1998) *J. Cell. Physiol.* **176,** 365–373
11. Ubl, J. J., Grishina, Z. V., Sukhomlin, T. K., Welte, T., Sedehizade, F., and Reiser, G. (2002) *Am. J. Physiol. Lung Cell Mol. Physiol.* **282,** L1339–L1348
12. Molino, M., Blanchard, N., Belmonte, E., Tarver, A. P., Abrams, C., Hoxie, J. A., Cerletti, C., and Brass, L. F. (1995) *J. Biol. Chem.* **270,** 11168–11175
13. Renesto, P., Si-Tahar, M., Moniatte, M., Balloy, V., Van Dorsselaer, A., Pidard, D., and Chignard, M. (1997) *Blood* **89,** 1944–1953
14. Kuliopulos, A., Covic, L., Seeley, S. K., Sheridan, P. J., Helin, J., and Costello, C. E. (1999) *Biochemistry* **38,** 4572–4585
15. Norton, K. J., Scarborough, R. M., Kutok, J. L., Escobedo, M. A., Nannizzi, L., and Coller, B. S. (1993) *Blood* **82,** 2125–2136
16. Déry, O., Corvera, C. U., Steinhoff, M., and Bunnett, N. W. (1998) *Am. J. Physiol.* **274,** C1429–C1452
17. Shpacovitch, V., Feld, M., Bunnett, N. W., and Steinhoff, M. (2007) *Trends Immunol.* **28,** 541–550
18. Hansen, K. K., Saifeddine, M., and Hollenberg, M. D. (2004) *Immunology* **112,** 183–190
19. Compton, S. J., Sandhu, S., Wijesuriya, S. J., and Hollenberg, M. D. (2002) *Biochem. J.* **368,** 495–505
20. Compton, S. J., Renaux, B., Wijesuriya, S. J., and Hollenberg, M. D. (2001) *Br. J. Pharmacol.* **134,** 705–718
21. Compton, S. J. (2003) *Drug Dev. Res.* **59,** 350–354
22. Opdenakker, G., Rudd, P. M., Ponting, C. P., and Dwek, R. A. (1993) *FASEB J.* **7,** 1330–1337
23. Wheatley, M., and Hawtin, S. R. (1999) *Hum. Reprod. Update* **5,** 356–364
24. Soto, A. G., and Trejo, J. (2010) *J. Biol. Chem.* **285,** 18781–18793
25. Tordai, A., Brass, L. F., and Gelfand, E. W. (1995) *Biochem. Biophys. Res. Commun.* **206,** 857–862
26. Mize, G. J., Harris, J. E., Takayama, T. K., and Kulman, J. D. (2008) *Protein Expr. Purif.* **57,** 280–289
27. Brass, L. F., Vassallo, R. R., Jr., Belmonte, E., Ahuja, M., Cichowski, K., and Hoxie, J. A. (1992) *J. Biol. Chem.* **267,** 13795–13798
28. Brass, L. F., Pizarro, S., Ahuja, M., Belmonte, E., Blanchard, N., Stadel, J. M., and Hoxie, J. A. (1994) *J. Biol. Chem.* **269,** 2943–2952
29. Sokolova, E., and Reiser, G. (2007) *Pharmacol. Ther.* **115,** 70–83
30. Ramachandran, R., Sadofsky, L. R., Xiao, Y., Botham, A., Cowen, M., Morice, A. H., and Compton, S. J. (2007) *Am. J. Physiol. Lung Cell Mol. Physiol.* **292,** L788–L798
31. Sambrano, G. R., Huang, W., Faruqi, T., Mahrus, S., Craik, C., and Coughlin, S. R. (2000) *J. Biol. Chem.* **275,** 6819–6823
32. Rao, N. V., Wehner, N. G., Marshall, B. C., Gray, W. R., Gray, B. H., and Hoidal, J. R. (1991) *J. Biol. Chem.* **266,** 9540–9548
33. Uehara, A., Sugawara, S., Muramoto, K., and Takada, H. (2002) *J. Immunol.* **169,** 4594–4603
34. Chen, X., Earley, K., Luo, W., Lin, S. H., and Schilling, W. P. (1996) *Biochem. J.* **314,** 603–611
35. Ubl, J. J., Sergeeva, M., and Reiser, G. (2000) *J. Physiol.* **525,** 319–330
36. Hamilton, J. R., Chow, J. M., and Cocks, T. M. (1999) *Br. J. Pharmacol.* **127,** 617–622